Spatially Resolved Measurement of Dynamic Glucose Uptake in Live Ex Vivo Tissues

Austin F. Dunn[†], Megan A. Catterton[†], Drake D. Dixon[†], Rebecca R. Pompano[‡]*

[†]Department of Chemistry

University of Virginia

PO BOX 400319

Charlottesville, VA 22904

Tel: 434-982-1825

[‡]Department of Chemistry

Carter Immunology Center

University of Virginia

PO BOX 400319

Charlottesville, VA 22904

*Corresponding author: rpompano@virginia.edu

ABSTRACT

Highly proliferative cells depend heavily on glycolysis as a source of energy and biological precursor molecules, and glucose uptake is a useful readout of this aspect of metabolic activity. Glucose uptake is commonly quantified by using flow cytometry for cell cultures and positron emission tomography for organs in vivo. However, methods to detect spatiotemporally resolved glucose uptake in intact tissues are far more limited, particularly those that can quantify changes in uptake over time in specific tissue regions and cell types. Using lymph node metabolism as a case study, we developed a novel assay of dynamic and spatially resolved glucose uptake in living tissue by combining ex vivo tissue slice culture with a fluorescent glucose analogue. Live slices of murine lymph node were treated with the glucose analogue 2-[N-(7-nitrobenz-2-oxa-1,3-dia-xol-4-yl)amino]-2-deoxyglucose (2-NBDG). Incubation and washing parameters were optimized to differentiate glucose uptake in activated versus naïve lymphocytes. Confocal microscopy of treated tissues confirmed that the 2-NBDG signal was intracellular. The assay was readily multiplexed with live immunofluorescence labelling to generate maps of 2-NBDG uptake across tissue regions, revealing highest uptake in T cell-dense regions. Uptake was predominantly localized to lymphocytes rather than stromal cells. Because 2-NBDG washed out of the tissue over time, the assay was repeatable in the same slices before and after T cell activation to reveal which tissue regions were most responsive to stimulation. We anticipate that this assay will serve as a broadly applicable, user-friendly platform to quantify dynamic metabolic activities in complex tissue microenvironments.

INTRODUCTION

This paper describes a novel, spatially-resolved assay of glycolytic activity in live, intact tissue, and demonstrates its use to quantify metabolic responses to ex vivo stimulation. Glycolysis is a highly conserved metabolic pathway that converts glucose to lactate and two ATP molecules.[1] This pathway is strongly upregulated in many cell types during periods of rapid proliferation, including cancer cells (Warburg effect), stem cells, and activated immune cells, even in the presence of oxygen.[2,3] While aerobic glycolysis is inefficient in terms of ATP production, it produces precursors of lipids, nucleotides, and proteins rapidly enough to meet heavy metabolic demands.[4]

The uptake of a glucose derivative is a common measure of glycolysis.[5] In particular, radiolabeled fluorodeoxyglucose (FDG) has a long history for in vivo analysis, and 2-[N-(7-nitrobenz-2-oxa-1,3-dia-xol-4-yl)amino]-2-deoxyglucose (2-NBDG) has been used more recently for fluorescent assays ex vivo and in vitro.[5,6] These molecules are only slightly larger than glucose alone and are readily imported through ubiquitously expressed GLUT receptors for glucose.[7,8] Studies of 2-NBDG indicate that phosphorylation of the probe by hexokinase, the first enzyme in the glycolytic pathway, traps the green-fluorescent molecule in the cell (Fig. 1a).[9] It remains there until it is either degraded to a non-fluorescent derivative or dephosphorylated to exit the cell. Thus, the intracellular fluorescent intensity of 2-NBDG provides an estimate of glucose uptake and initial processing that can be detected by flow cytometry or fluorescent microscopy.[5,10,11]

Most assays of glucose uptake are conducted in vitro or in vivo, settings that offer powerful insights but are limited in their ability to provide dynamic metabolic information. Assays using cell suspensions enable well-controlled stimulation and are readily analyzed in high throughput by flow cytometry. However, cell positioning and cell-cell interactions are thought to be essential to

tissue function, and these are challenging to reproduce in vitro.[12–15] In vivo analysis of glucose uptake, on the other hand, detects metabolic activity in situ with minimal perturbation, making it a powerful diagnostic for cancer and inflammation.[16–19] However, it can be difficult to deliver controlled stimulation or determine cellular phenotypes in vivo in the absence of genetic reporters. As a complementary approach, measuring ex vivo glucose uptake in live tissue sections generates spatially resolved readouts of metabolic activity, which have been used to identify cancerous tissues based on universally high glucose uptake, as well as visualize single-cell uptake of glucose analogues within mouse brain slices.[19–23] However, so far, no methods exist to measure dynamic glucose uptake ex vivo in response to well controlled stimulation, making it difficult to quantify glycolytic responses in heterogeneous tissues.

A major challenge in comparing glucose uptake between highly organized tissues is high biological variability in basal glucose uptake, both within and between tissue samples. Large intra-group variability can dwarf small inter-group differences, making it difficult to power experiments adequately.[24] In this context, performing before-and-after measurements within each sample, e.g., in response to stimulation, sets up each sample as its own control. This approach, called repeated-measures experimental design, greatly improves the statistical power of the experiment and reduces the number of samples required.[25] Use of this experimental design requires that the assay have minimal effect on tissue health and activity even when performed repeatedly.

Dynamic glucose uptake is particularly interesting in the context of immunology,[26–30] a system characterized by spatial organization within heterogeneous tissues.[31–34] The growing field of immunometabolism utilizes measures of metabolic activity to predict immune cell development, differentiation, and activation, and to pinpoint therapeutic targets for immunomodulation.[35–37] Glucose uptake has been correlated with the activation state of T cells, B cells, and antigen-

presenting cells, both in tumor immunology and in the response to vaccination.[38,39] However, these assays were performed mainly at the cellular level, and it is not yet clear how glycolytic activity is distributed throughout immune tissues such as the lymph node. The lymph node is a highly structured organ, and its sub-structures vary widely in terms of cellular composition and activity.[40,41] The spatial distribution of glucose uptake in the lymph node is not known in resting nodes nor during an immune response.

Here, we report a new method to quantify spatially resolved glucose uptake in live tissue slices, taking advantage of 2-NBDG as a fluorescent probe and validating a repeated-measures approach to measuring the metabolic response to ex vivo stimulation (Fig. 1b). The assay was designed to be compatible with most soft tissues (e.g., brain, lung, tumors). We applied 2-NBDG in combination with live immunofluorescent staining to whole, 300 µm-thick slices of live lymph node tissue,[42] to reveal metabolic heterogeneity and region-specific responses to activation (Fig. 1c).

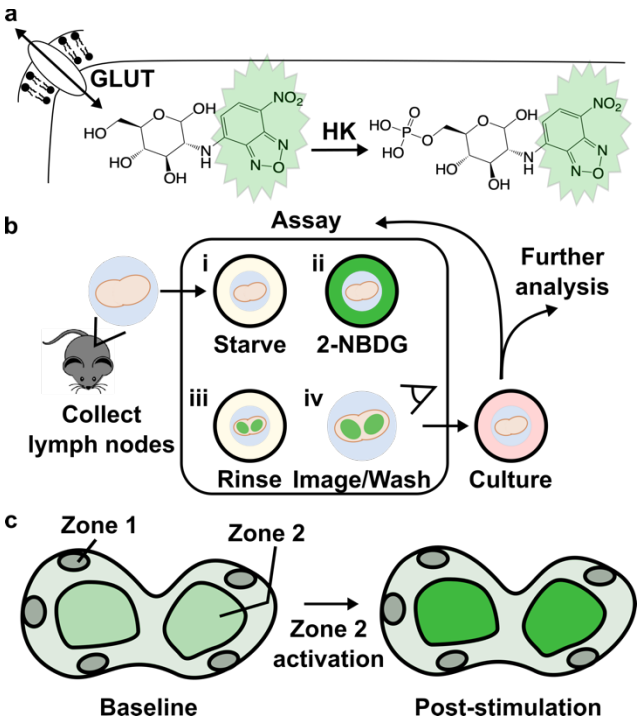

Figure 1. Design of an e*x vivo* metabolic assay to visualize glucose uptake in live tissue. (a) 2-NBDG is imported through the same GLUT receptors as glucose and temporarily trapped within cells by hexokinase (HK)-mediated phosphorylation. (b) Schematic of assay procedure, which includes a glucose-starvation step, incubation with 2-NBDG and brief rinse, and imaging of the labelled tissue. The assay may be repeated before and after a culture step as needed. Further analysis such as antibody labeling can be performed on the live tissue after 2-NBDG wash-out. (c) Schematic of a heterogeneous tissue sample, showing hypothetically varied basal 2-NBDG uptake (green shading), and potentially region-specific responses following stimulation.

EXPERIMENTAL SECTION

Animal care. All animal work was approved by the Institutional Animal Care and Use Committee at the University of Virginia under protocol #4042, and was conducted in compliance with guidelines from the University of Virginia Animal Care and Use Committee and the Office of Laboratory Animal Welfare at the National Institutes of Health (USA). Male and female C57BL/6 mice were purchased from Jackson Laboratories and used while 6-12 weeks old. Mouse were housed in a vivarium under 12-hour light/dark cycles and given food and water *ad libitum*.

Flow cytometry. Analysis was performed on pooled inguinal, brachial, and axillary lymph nodes from 1 female mouse and 1 male mouse after humane sacrifice via isoflurane overdose and cervical dislocation. Lymph nodes were crushed through a 70-µm filter and centrifuged (Sorvall ST40R Centrifuge, Fisher Scientific) at 400 x g for 5 min. Lymphocytes were cultured at $1x10^6$ cells/mL in culture-treated 96-well plates in complete media. Complete media consisted of RPMI 1640 without L-glutamine (Lonza), supplemented with 10% fetal bovine serum (FBS), 1% l-glutamine, 1% Pen-Strep, 50 µM beta-mercaptoethanol, 1 mM pyruvate, 1% non-essential amino acids, and 20 mM HEPES (Fisher Scientific). For stimulation experiments, cells were cultured overnight with or without 4 µg/mL Syrian hamster anti-mouse CD28 (clone 37.51, BioLegend, USA) and plate-bound Armenian hamster anti-mouse CD3ε (clone 145-2C11, BioLegend, USA, coated using 10 µg/mL in PBS overnight at 4°C). Cells were collected, centrifuged, rinsed once in PBS with 2% serum (VWR), and resuspended in a "starve media" (PBS with 10% serum). 2-NBDG (Thermo Fisher) was prepared in 20 mM aliquots in DMSO and stored at -20°C. 2-NBDG was spiked into the starve media at the indicated concentration (25, 100, or 200 µM) and incubated at 37°C and 5% CO_2 for the indicated time (15, 30, or 45 min). Following 2-NBDG treatment, all cell suspensions were Fc blocked with rat anti-mouse CD16/32 (clone 93, BioLegend, USA) and then stained with 10 µg/mL AlexaFluor647 Armenian hamster anti-mouse CD3ε (clone 145-2C11, BioLegend, USA) followed by 0.5 µg/mL 7-AAD (AAT Bioquest). Single-stain and FMO (fluorescence-minus-one) control conditions were set up as appropriate. For a killed control, 35% EtOH was added to a cell suspension for 20 min at room temperature. Data were collected using a Millipore Sigma Guava easyCyte 6-2L flow cytometer, acquiring data using GuavaSoft 3.3 software. Compensation and data analysis were performed using FCS Express 6 software after

gating the cells on scatter. Compensation matrices were calculated based on median fluorescent intensity of controls. Median intensity was reported for all samples.

Slice Preparation and Culture. Tissue slicing was performed as previously described.[42,43] In brief, mice were humanely sacrificed, and inguinal, brachial, and axillary lymph nodes were removed and submerged in ice-cold complete media. Tissues were embedded in 6% low-melting point agarose (Lonza) for two minutes on ice. Agarose blocks were sliced to 300 µm thickness using a vibratome (Leica VT1000S) under sterile conditions. Immediately after slicing, tissue slices were incubated in 1 ml/slice pre-warmed Complete media at 37°C/5% CO_2 for one hour to recover. Where noted in experiments, the media was spiked with phytohaemagglutinin-L (PHA-L) (Millipore Sigma) at a concentration of 25 µg/mL during culture.

Widefield Imaging. For all imaging steps, slices were transferred into a 12-well plate in 0.5 mL PBS for immediate imaging on an upright AxioZoom macroscope using a HXP 200 C metal halide lamp, PlanNeoFluor Z 1x/0.25 FWD 56 mm objective, and Axiocam 506 mono camera (Carl Zeiss Microscopy). Filters used were Zeiss Filter Set 38 HE (Ex: 470/40, Em: 525/50), 43 HE (Ex: 550/25, Em: 605/70); 64 HE (Ex: 587/25, Em: 647/70); and 50 HE (Ex: 640/30, Em: 690/50). Brightfield images were also collected for each slice with 10 ms exposure. All fluorescent images of antibody staining were collected at 900 ms. 2-NBDG imaging used 300 ms exposure and filter 38 HE ("FITC"). Zen 2 blue software was used for image collection.

Confocal imaging. After slices had been imaged on widefield microscope, they were immediately returned to ice and transported to a Nikon A1R Confocal microscope. One slice at a time was

mounted onto a glass slide and a coverslip was placed on top. A 10x objective was used to locate regions of interest, then slices were imaged with a NIR Apo 40x 0.8W DIC N2 objective. Wavelengths (in nm) of the lasers and filters used were 487 (Emission filter: 525/50), 561 (Emission filter: 595/50), 638 (Emission filter: 700/75). Laser power used for imaging was 0.5, and gain was adjusted for each channel – 95 (FITC), 110 (TRITC), 135 (Cy5). All images were collected between approximately 10-30 μm depth into tissue.

2-NBDG Assay Procedure. A 2-NBDG working solution was prepared fresh for each experiment, consisting of 100 μM 2-NBDG in "starve media" (PBS + 10% FBS); this solution was stored at 4°C when not in use. Staining with 2-NBDG was similar to previously published live lymph node slice staining procedures with other reagents.[44] First, to record baseline autofluorescence, lymph node slices were rinsed once with 1x PBS and imaged in a tissue culture treated 12-well plate as described above. The PBS was removed and replaced with 900 μL of pre-warmed starve media, and the slices were incubated 30 min (37°C with 5% CO_2). Next, a 6-well plate was prepared by lining the wells with paraffin film to provide a hydrophobic surface. A 30 μL droplet of the 2-NBDG solution was placed on the parafilm, a tissue slice was carefully transferred on top using a fan brush and weighed down with an A2 stainless steel flat washer (10 mm outer diameter, 5.3 mm inner; Grainger, USA), and another 30 μL droplet of 2-NBDG was added on top to ensure staining on both the sides of the tissue. The 6-well plate was covered and incubated for 30 min (37°C with 5% CO_2). Next, slices were rinsed by soaking in 1.5 mL 1x PBS per slice for 15 min (4°C), shaking gently halfway through the rinsing period. Slices were transferred to 0.5 mL chilled 1x PBS and immediately imaged. Slices were returned to complete media and incubated (37°C with 5% CO_2)

pending further use. Care was taken not to flip the slices over at any point during the assay procedure.

Immunostaining of live lymph node slices. Live fluorescence immunostaining was performed according to previously published methods.[44] Briefly, live slices were transferred placed on parafilm, Fc-blocked for 30 min, and labelled with an antibody cocktail for one hour. Antibodies used were FITC-rat anti-mouse/human CD45R/B220 (clone RA3-6B2, BioLegend), and rat anti-mouse CD4 $F(ab')_2$ fragment (clone GK1.5, BioLegend, fragmented according to published procedures[45]) that was conjugated using AlexaFluor 594-succinimidyl ester according to manufacturer instructions (Thermo Fisher). All antibodies were used at a concentration of 20 µg/mL (0.2 µg per tissue slice). Slices were rinsed for 1 hr in PBS to remove unbound antibodies.

Image Analysis. Images of slices were analyzed using Fiji v1.48.[46] T cell rich regions-of-interest (T cell zone ROI; $CD4^+B220^-$) were identified manually from immunofluorescence images, by a researcher who was blinded to the images with 2-NBDG. Images of 2-NBDG were then rotated and translated to match the orientation of the tissue in the antibody stained images, and the traced regions of interest were copied onto them. The mean fluorescent intensity (MFI) of 2-NBDG signal was quantified in the T cell zone ROI and, separately, in the areas of tissue excluded from that ROI ("non-T cell zone"). Where noted, the entire slice was traced instead, by identifying the border based on brightfield images. 2-NBDG intensity (2-NBDG Int.) values are reported with autofluorescence subtracted out, as follows,

$$\text{2-NBDG int.} = \left(ROI\ int._f - background\ int._f\right) - \left(ROI\ int._i - background\ int._i\right) \qquad (1)$$

where "*i*" (initial) represents the intensity prior to 2-NBDG treatment (i.e., autofluorescence) and "*f*" (final) represents the intensity measured after the assay with 2-NBDG. "Background int." for each image was defined as the average of three regions of the image not containing tissue. Slices that had little T cell zone, defined as fewer than 1.5×10^5 μm^2 contiguous area, were excluded from analysis. For 2-NBDG image display, brightness and contrast were adjusted uniformly across all slices that are displayed in the same figure.

Statistics. Statistical tests and curve fits were performed in GraphPad Prism 8.3.0.

RESULTS AND DISCUSSION

Optimization of 2-NBDG treatment to detect T cell activation in mixed cultures

Our goal was to develop an assay that could detect increased glucose uptake in a lymph node undergoing glycolysis-inducing immune activation.[26] In preliminary experiments using unoptimized labelling conditions, we observed that the intensity and distribution of the 2-NBDG signal was similar between live and ethanol-killed samples (data not shown), indicating that a substantial portion of the 2-NBDG uptake was not driven by metabolic processes.[10] Therefore, we sought to identify conditions that maximized the sensitivity to 2-NBDG uptake due to active metabolism, not just passive diffusion or non-specific binding.[47]

To distinguish activated from resting lymphocytes, we performed time-course and concentration optimization experiments for 2-NBDG similar to those previously conducted on other cell types.[11,48–50] 2-NBDG treatment was conducted in a "starve media" consisting of PBS containing 10% FBS to limit the amount of D-glucose, which could out-compete 2-NBDG for uptake,[9] while providing some minimal nutrients and proteins.[51] Mixed murine lymphocytes were

used to approximate the lymphocyte distribution and any cell-cell interactions present in the lymph node tissues. Cells were cultured overnight with or without T cell stimulation by anti-CD3 and anti-CD28. For analysis by flow cytometry, the population was gated on live cells that were CD3-positive and/or expanded in size (higher forward scatter), to identify resting and activated T cells (Fig. 2a-c). We note that this gating strategy, necessitated by the internalization of CD3 after anti-CD3 stimulation,[52] may capture any large $CD3^-$ cells as well.

The ability to distinguish activated from naïve T cells depended strongly on the incubation conditions (Fig. 2e-g). Even formalin-fixed lymphocytes were labelled by 2-NBDG, suggesting that small amounts of 2-NBDG diffused passively into or adhered to the surface of non-viable cells (Fig. 2g). After a short 2-NBDG treatment (15 min, 100 μM), live cells showed a single peak that was indistinguishable between naïve and stimulated conditions (Fig. 2d), and the signal often overlapped with that of fixed controls (not shown), suggesting at this time point, the signal was due to passive labelling rather than quantifiable metabolic activity. In contrast, after 30-min 2-NBDG treatment, a new peak appeared in the stimulated condition, creating a characteristic "doublet" pattern with two closely overlapping peaks (Fig. 2e). The 1.3-fold difference in intensity between the two peaks, though small, was consistent with prior reports showing a 1.3 – 2.0-fold increase in 2-NBDG uptake by T cells after metabolic stimulation (Fig. 2h).[27,49] We concluded that the brighter peak represented increased retention of 2-NBDG driven by stimulation-induced metabolism. In a separate experiment, inclusion of high D-glucose concentrations (11 mM in RPMI versus ~700 μM in the starve media) during 2-NBDG treatment prevented the appearance of the brighter peak, consistent with the requirement for uptake via glucose receptors expected in mammalian cells (Figure S1).[9,10] For reference, physiological blood glucose levels average 9.1 mM in C57Bl/6 mice.[53] Lower concentrations of 2-NBDG (25 μM) produced only low-intensity

singlet peaks, with no detectable effect of stimulation (Fig. 2h). Finally, in agreement with reports in kidney and heart cells,[54,55] we observed evidence of saturation of 2-NBDG uptake at longer times (45 min) (Fig. 2f) and higher concentrations (200 μM) (Fig. 2h). Under each of these conditions, even naïve cells featured the doublet pattern and the median fluorescent intensity levelled off. As the response to stimulation was best detectable after 30 min staining with 100 μM 2-NBDG, this condition was selected as the appropriate condition to test in lymphoid tissue.

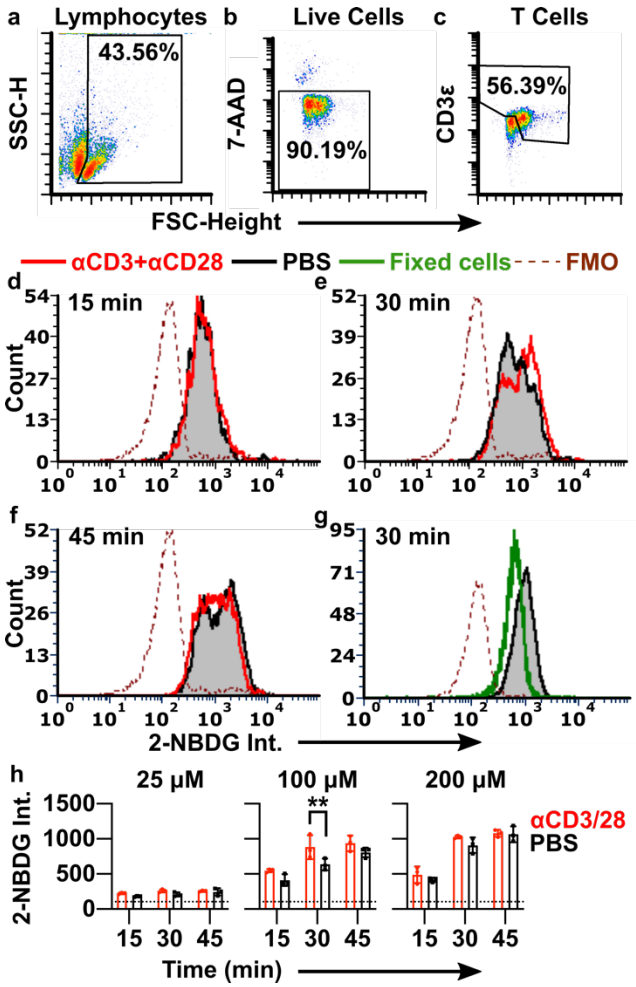

Figure 2. Optimization of 2-NBDG labelling conditions to detect T cell activation. (a-c) Mixed murine lymphocytes were gated on scatter (a), singlets (not shown), 7-AAD exclusion (b), and a combination of high expanded forward scatter and CD3 expression to identify resting and activated T cells (c). SSC-H shown on linear scale; 7-AAD and CD3 intensities shown on log scale. (d-g) 2-NBDG histograms after cells were stimulated with anti-CD3+anti-CD28 (red) or left unstimulated (black) and treated with 100 μM 2-NBDG for 15 min, 30 min, or 45 min. Dotted line is the fluorescence-minus-one (FMO) control for 2-NBDG. Histograms normalized to 5000 events. (g) 2-NBDG labeling of live and formalin-fixed cells after 30 min, 100 μM 2-NBDG. Fixed samples gated on singlet events. (h) Median 2-NBDG intensity (int.) depended on incubation time and concentration of 2-NBDG. Bars show mean ± std dev of N=3 replicates. Dotted lines show mean of FMO (no 2-NBDG) control. Two-way ANOVA with Sidak's multiple comparisons, ** represents $p<0.01$.

Establishing conditions for 2-NBDG labeling and repeated analysis in live tissue

Unlike analysis in cell culture, analysis of glucose uptake in thick slices of tissue required consideration of tissue-specific properties: restricted mass transport (slow diffusion), potential for non-specific binding to the matrix, and tissue heterogeneity and autofluorescence. Because of

restricted transport, insufficient rinsing could lead to high residual 2-NBDG signal, not reflective of metabolic activity, so we tested short (2 min) and long (15 min) rinse times. Slices were killed with EtOH to halt metabolic activity as a negative control. After a 2 min rinse, the intensities of live and killed slices were similar (Fig. 3a, Fig. S2). After a 15 min rinse, 2-NBDG signal had decreased significantly in killed slices but not in live slices, and signal in killed slices was not significantly above background (one sample t test, $p<0.05$ denotes significance). Therefore, we concluded that a 15 min rinse was adequate to remove most residual 2-NBDG. This result agreed with theoretical estimates for diffusion of 2-NBDG. Using the range of diffusive properties of glucose in the brain and eye as a rough estimate (D = ~0.91 x 10^{-6} - 2.6 x 10^{-6} cm^2/s)[56], 2-NBDG that has not been transported into cells should travel through a 300 µm thick tissue slice in ~3-8 min ($x^2 = 2Dt$, where x is distance [cm] and t is time [s]). To confirm that the signal in live tissues was not due to matrix binding, live slices labelled under these conditions (100 µM, 30 min incubation, 15 min rinse) were imaged by confocal microscopy. The 2-NBDG signal appeared primarily intracellular rather than matrix-bound, with well-defined bright circular regions consistent with the dimensions of lymphocytes (Fig. 3b), and was substantially brighter than in unstained controls (data not shown).

Unlike well mixed cell suspensions, tissue slices are likely to contain significant cellular heterogeneity within and between samples, both in terms of metabolic activity and autofluorescence. Indeed, widefield fluorescence imaging revealed clearly defined regions of high and low 2-NBDG uptake across the naïve lymph node slices (Fig. 3c), which was clearly distinguishable from tissue autofluorescence (Fig. 3d). The mean 2-NBDG intensity varied by up to 5-fold between lymph node slices (Fig. 3e), consistent with the fact that each tissue slice contains a unique combination and number of lymphocytes and other cell types, likely at varied density and

with varied permeability of the extracellular matrix.[42] This variability, coupled with the expected small change in 2-NBDG uptake upon stimulation (< 1.5-fold, Figure 2), led us to the conclusion that a repeated-measures experimental design, in which the same tissue would be measured before and after stimulation, would be far more powerful than comparing separate groups of stimulated versus unstimulated slices.

To enable repeated analysis of the same tissue slice, we characterized the minimum recovery time needed for the 2-NBDG signal to decay (Fig. 3f). Based on prior reports, decay of cellular 2-NBDG signal over time is due to a combination of dephosphorylation and export of 2-NBDG and intracellular decomposition into a non-fluorescent form.[7] After 30-min incubation with 2-NBDG and a 15-min rinse, tissues were cultured in complete media at 37 °C, 5 % CO_2 and imaged periodically. The 2-NBDG signal diminished by >85% after 2 hr. Based on these results, in future experiments we waited at least 2 hr before repeating the assay, and collected a new "initial" image immediately prior to each 2-NBDG treatment to ensure that any residual 2-NBDG was properly subtracted (Equation 1).

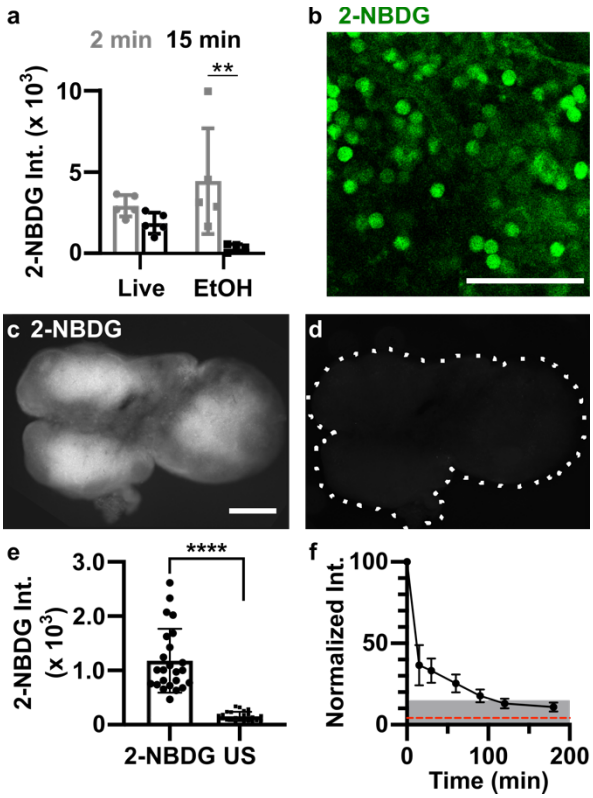

Figure 3. Applying 2-NBDG for quantitative analysis in live tissue. (a) Mean 2-NBDG intensity of live and EtOH-treated slices after two different rinse times (N=5 slices). Slices were imaged at 2 min and again at 15 min. Pixel intensity was averaged over whole tissue area in widefield images after subtracting autofluorescence (Eq. 1). Two-way ANOVA with Sidak's multiple comparisons, ** represents $p<0.01$. (b) Representative confocal image of 2-NBDG staining in live slices of naïve lymph node. 2-NBDG applied 30 min, 100 µM. Tissue imaged at a depth of 20-30 µm. Scale bar 50 µm. (c) Representative widefield image of 2-NBDG staining in a live naïve lymph node slice. Scale bar 500 µm. (d) Image of the same slice prior to 2-NBDG labelling, showing minimal autofluorescence (same brightness and contrast). Dotted line shows slice border. (e) Mean 2-NBDG intensity in naïve slices with or without 2-NBDG staining (US, unstained). Bars show mean ± standard deviation, N=24. **** represents $p<0.0001$ by paired t-test. (f) Normalized 2-NBDG intensity, measured over time as slices were incubated in media after a single staining step (N=7 slices). Mean intensity data from each slice were normalized to the intensity of that slice at t=0 min. Dotted red line shows mean intensity of unstained slices. Shaded area represents less than 15% of original signal remaining.

Mapping spatially resolved 2-NBDG uptake in tissue

To interpret the spatial distribution of 2-NBDG uptake in lymph node slices, we followed the 2-NBDG assay with live immunofluorescence labelling to identify two regions of interest – the deep paracortex, also referred to as the T cell zone ($CD4^{high}B220^{low}$), and the remainder, which includes B cell follicles ($B220^{high}$ circular zones) and sinuses ($B220^{med}$) (Fig. 4a).[44] We observed that in

naïve tissues, T cell zones appeared significantly brighter than in the small B cell follicles or sinus regions (Fig. 4b-d, Fig. S3). In fact, B cell follicles were often clearly apparent as darkened patches on the slice periphery in the 2-NBDG image. B cell follicles, like the rest of the lymph node, are densely packed with cells, suggesting that cell density was not the driving force behind the difference in glucose uptake.[57]

The bright signal observed in the T cell zone could be due to T cells ($CD4^+$ or $CD8^+$), the supporting stromal fibroblasts (podoplanin-expressing fibroblastic reticular cells, FRCs), or less abundant antigen presenting cells. To determine which cell types contributed the most to the 2-NBDG signal in the T cell zone, the lymph node slice was pre-labelled with fluorescent antibodies for cell surface markers, and treated with 2-NBDG immediately afterwards. This imaging strategy allowed for immunofluorescence and glucose uptake to be analyzed simultaneously, avoiding the need for repeated imaging of the tissue. Central regions high in 2-NBDG uptake were identified by widefield imaging and then analyzed further by confocal microscopy (Fig. 4e). Cell surface staining of CD4 and CD8 formed roughly circular outlines, some of which bounded a circular 2-NBDG bright region, and some of which were dark inside (no detectable 2-NBDG uptake). Of the 2-NBDG-bright regions, most (71%) were surrounded by staining for either CD4 or CD8 (Fig. 4f), suggesting that they were T cells. We considered the possibility that the remaining 2-NBDG-high cells ($CD4^-CD8^-$) could be a stromal population. However, the FRC marker podoplanin showed minimal overlap with 2-NBDG (Fig. 4g), indicating that these cells did not contribute to the 2-NBDG positive population in the slices. The identity of the $CD4^-CD8^-$ cells was not further investigated here. In summary, these experiments showed that simple incubation with 2-NBDG could reveal spatially heterogeneous glucose uptake in live tissues, and that coupling with live

immunofluorescence could provide phenotyping of glucose-rich regions at the whole-tissue and cellular length scales.

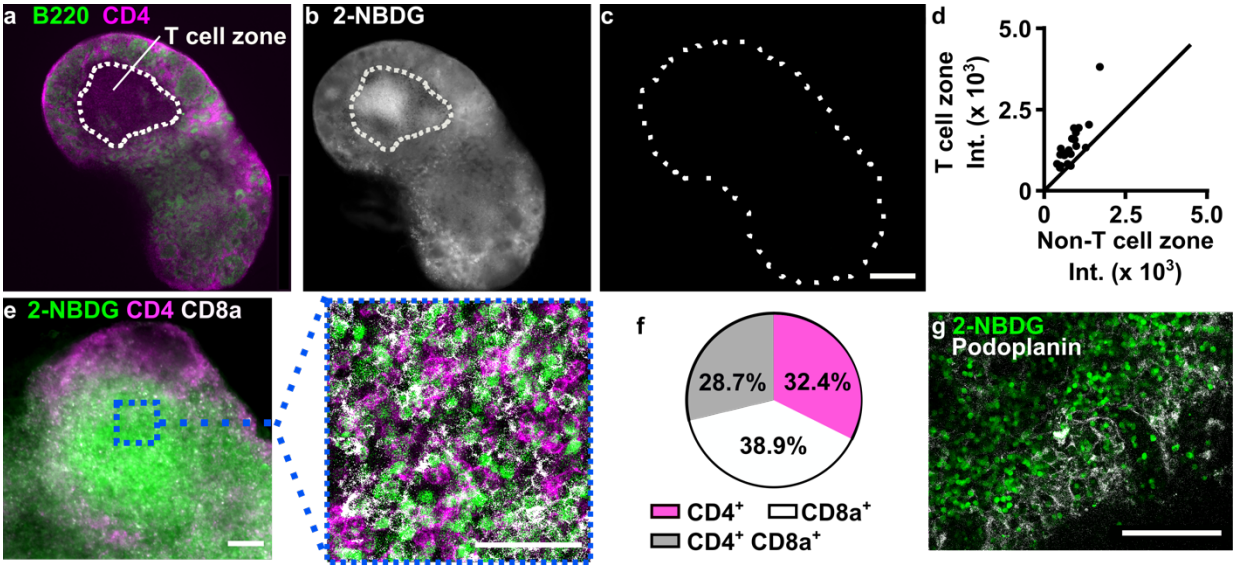

Figure 4. Spatial distribution of 2-NBDG uptake coupled with immunofluorescence. (a) Representative widefield immunofluorescence image of a naïve lymph node slice. Outline represents blinded tracing of T cell zone ($CD4^+B220^-$ area). (b-c) Images from (b) 2-NBDG staining and (c) prior to staining in the same slice. Dotted line shows slice border. 2-NBDG images scaled to same brightness and contrast. Scale bar 500 µm. (d) Region-specific mean 2-NBDG intensity within naïve lymph node slices. Intensity was measured inside and outside of T cell zones ($CD4^+B220^-$). y=x line plotted for reference. Each dot represents one slice. (e) Representative paired widefield and confocal images of lymph node slice after live immunostaining and 2-NBDG assay. Left scale bar 100 µm, right 50 µm. Individual cells positive for 2-NBDG uptake were visible in confocal images. (f) Manual cell counts determined the percentage of 2-NBDG-positive cells in the T cell zones that were co-stained with CD4, CD8, or neither. Data compiled from N=11 tissue slices from three mice. (g) 2-NBDG uptake overlaid with immunofluorescence for podoplanin, a surface marker for lymphoid stroma. Representative of N=7 slices from two mice. Scale bar 100 µm.

Quantifying local changes in 2-NBDG uptake following metabolic stimulus

Having shown that a single round of the 2-NBDG assay could map out the distribution of glucose uptake, we next addressed the challenge of quantifying responses to ex vivo stimulation over time. As discussed above, both cell compositions and basal metabolic rates vary widely between tissue slices (Fig. 3e), and this variance could mask small changes in glucose uptake between stimulated

and unstimulated tissues. We reasoned that the effects of phenotypic variability could be minimized by using a repeated measures experimental design.

To test this hypothesis, we performed the 2-NBDG assay repeatedly in single tissue slices, before and after a metabolic activator was applied. In this manner, each slice served as its own control, thus accounting for the variation in basal metabolic activity within and between slices. Phytohemagglutinin (PHA) stimulation was used to induce a rapid change in metabolic state. PHA crosslinks glycosylated surface receptors such as the T cell receptor (TCR), leading to upregulation of glycolysis within 3 hours, particularly in the T cell population.[58–61] Murine T cells stimulated via the TCR upregulate surface GLUT1 receptors within 2-4 hr, an early hallmark of T cell activation.[62] Additionally, increased hexokinase activity has been observed after 2 hr PHA stimulation of mixed lymphocytes.[63] We therefore hypothesized that a 3-hour culture with PHA would increase 2-NBDG uptake primarily in the T cell zone, and would be sufficient to clear the majority of the 2-NBDG after the first round of the assay (Fig. 3f). Autofluorescence and basal 2-NBDG uptake were assayed as above, and then the lymph node slices were cultured with or without PHA for 3 hours. After the culture period, the 2-NBDG assay was repeated, and finally the slices were immunostained for B220 and CD4 to define the tissue architecture (Fig. 5a-h, Fig. S3). The immunostaining step was performed last to avoid antibody-mediated T cell activation during the multi-hour culture period.[44]

Basal 2-NBDG uptake was greatest in the T cell zone ($CD4^{high}$ $B220^{low}$ regions), with the remaining regions – a composite of B cell follicles, sinuses, and macrophage-rich medulla – remaining dark. As expected, ex vivo PHA stimulation produced a response that was detectable across the entire tissue on average (Fig. S4), and the response was localized specifically to the T cell zones. Quantitative image analysis showed a small increase in 2-NBDG uptake in the T cell

zone after PHA stimulation (1.26-fold ± 0.27, mean ± stdev, N = 11 slices; Fig. 5i) that was significantly different than the response to media control. The magnitude of the response was consistent with cellular responses observed by flow cytometry in Figure 2, with variability characteristic of tissue slices. In contrast, locations outside of the T cell zone did not respond on average (1.03-fold ± 0.22, mean ± stdev, N = 11 slices; Fig. 5j) and were not significantly different than media controls. Notably, the media controls exhibited unchanged or even slightly diminished 2-NBDG uptake during the 3-hr culture (e.g., 0.90-fold ± 0.21 in T cell zones mean ± stdev, n = 11 slices; Fig. 5i), indicating perhaps a small change in basal metabolic activity during culture of lymph node slices; this phenomenon remains to be further explored. In summary, these data demonstrate that the 2-NBDG assay can reveal changes in metabolic activity over time in live tissue with regional specificity, including the response to ex vivo stimulation.

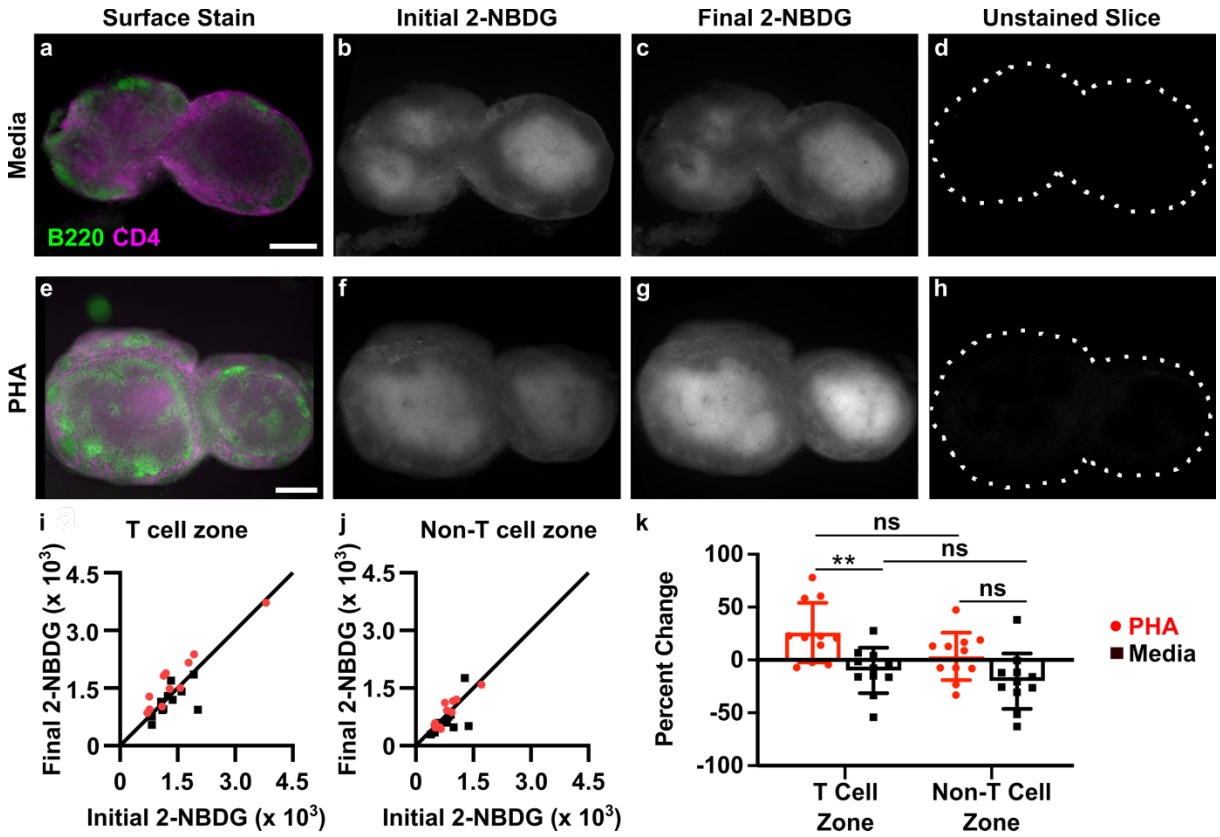

Figure 5. Analysis of local changes in glucose uptake in a repeated-measures experiment. (a-h) Representative images of lymph node slices cultured in media as a negative control (a-d) or with 25 µg/ml PHA (e-h). (a,e) Immunofluorescence imaging to identify T cell zones, (b,f) initial 2-NBDG, (c,g) 2-NBDG following 3 hr culture, (d,h) initial unstained image. All 2-NBDG images are scaled to the same brightness and contrast. Scale bars 500 µm. (i,j) Quantification of mean 2-NBDG intensity in the (i) T cell zones and (j) non-T cell zones, before and after 3-hr culture with PHA or media control. y=x line plotted for reference; dots on the line show no change in 2-NBDG uptake after culture. Each dot represents one slice, N=11 slices. (k) Data plotted as percent change from initial to final 2-NBDG intensity (0% = no change, 100% = doubling of intensity). Two-way ANOVA with Sidak's multiple comparisons, ** represents $p<0.01$.

CONCLUSIONS

We have developed a novel imaging-based assay that generates quantitative, spatially resolved maps of glucose uptake in live tissues at multiple time points during ex vivo culture. The method is simple and robust, requiring only incubation and rinse steps with a commercially available fluorescent reagent, 2-NBDG. The 2-NBDG assay can be combined with live immunofluorescence labeling to determine which cell types internalize the most and least 2-NBDG. It can be used with

a repeated measures experimental design to detect spatially resolved responses to stimulation in individual tissue slices.

When applied to live slices of lymph node tissue, this approach revealed varied glycolytic activity across the lymph node, which was clearly distinct from autofluorescence. Ethanol-fixed controls demonstrated that rinsing was sufficient to remove non-specifically incorporated 2-NBDG from the lymph node tissue. The 2-NBDG signal was greatest in the paracortex (T cell zone), and ~70% of the signal could be attributed to $CD4^+$ or $CD8^+$ lymphocytes. When cultured with a T cell mitogen, the response was localized to the paracortex, as expected.

Compared to in vitro assays of glucose uptake, an ex vivo approach preserves the tissue microenvironment and provides insight into the organization of metabolically active cells. On the other hand, compared to in vivo glucose-sensing methods, ex vivo culture allows for more precise control over the timing and dose of stimulation in a particular organ. This method should be applicable to other types of soft tissue, and to models of disease that feature changes in glycolytic activity. Future work may leverage this method to characterize region-specific responses in diseased tissues and evaluate the effects of therapeutic agents.

ACKNOWLEDGEMENTS

We thank The Hartwell Foundation for generously funding this work and for helpful discussions on data analysis strategies. Research reported in this publication was supported by the University of Virginia 3Cavaliers Program through the Office of the Vice President for Research, and by the National Institute of Allergy and Infectious Diseases under Award Number R01AI131723 through the National Institutes of Health (NIH). The content is solely the responsibility of the authors and does not necessarily represent the official views of the National Institutes of Health. Some

equipment for this project was funded by a Starter Grant Award from the Society of Analytical Chemists of Pittsburgh. DDD was supported by a Department of Chemistry Summer Scholarship and the College Science Scholars Program. The authors thank Ms. Alexis Chernish for experimental contributions at early stages of this project.

References

(1) Kim, J.-W.; Dang, C. V. Multifaceted Roles of Glycolytic Enzymes. *Trends Biochem. Sci.* **2005**, *30* (3), 142–150.
(2) Lunt, S. Y.; Vander Heiden, M. G. Aerobic Glycolysis: Meeting the Metabolic Requirements of Cell Proliferation. *Annu. Rev. Cell Dev. Biol.* **2011**, *27* (1), 441–464. https://doi.org/10.1146/annurev-cellbio-092910-154237.
(3) Shyh-Chang, N.; Daley, G. Q.; Cantley, L. C. Stem Cell Metabolism in Tissue Development and Aging. *Development* **2013**, *140* (12), 2535–2547. https://doi.org/10.1242/dev.091777.
(4) Wang, R.; Green, D. R. Metabolic Reprogramming and Metabolic Dependency in T Cells. *Immunol. Rev.* **2012**, *249* (1), 14–26. https://doi.org/10.1111/j.1600-065X.2012.01155.x.
(5) TeSlaa, T.; Teitell, M. A. Techniques to Monitor Glycolysis. *Methods Enzymol.* **2014**, *542*, 91–114. https://doi.org/10.1016/B978-0-12-416618-9.00005-4.
(6) Strauss, L. G.; Conti, P. S. The Applications of PET in Clinical Oncology. *J. Nucl. Med.* **1991**, *32* (4), 623–648.
(7) Yoshioka, K.; Saito, M.; Oh, K. B.; Nemoto, Y.; Matsuoka, H.; Natsume, M.; Abe, H. Intracellular Fate of 2-NBDG, a Fluorescent Probe for Glucose Uptake Activity, in Escherichia Coli Cells. *Biosci. Biotechnol. Biochem.* **1996**, *60* (11), 1899–1901. https://doi.org/10.1271/bbb.60.1899.
(8) Sheth, R. A.; Josephson, L.; Mahmood, U. Evaluation and Clinically Relevant Applications of a Fluorescent Imaging Analog to Fluorodeoxyglucose Positron Emission Tomography. *J. Biomed. Opt.* **2009**, *14* (6). https://doi.org/10.1117/1.3259364.
(9) O'Neil, R. G.; Wu, L.; Mullani, N. Uptake of a Fluorescent Deoxyglucose Analog (2-NBDG) in Tumor Cells. *Mol. Imaging Biol.* **2005**, *7* (6), 388–392. https://doi.org/10.1007/s11307-005-0011-6.
(10) Yamada, K.; Saito, M.; Matsuoka, H.; Inagaki, N. A Real-Time Method of Imaging Glucose Uptake in Single, Living Mammalian Cells. *Nat. Protoc.* **2007**, *2* (3), 753–762. https://doi.org/10.1038/nprot.2007.76.
(11) Rajaram, N.; Frees, A. E.; Fontanella, A. N.; Zhong, J.; Hansen, K.; Dewhirst, M. W.; Ramanujam, N. Delivery Rate Affects Uptake of a Fluorescent Glucose Analog in Murine Metastatic Breast Cancer. *PLOS ONE* **2013**, *8* (10), e76524. https://doi.org/10.1371/journal.pone.0076524.
(12) Andrian, U. H. von; Mempel, T. R. Homing and Cellular Traffic in Lymph Nodes. *Nat. Rev. Immunol.* **2003**, *3* (11), 867. https://doi.org/10.1038/nri1222.

(13) Ben-Moshe, S.; Itzkovitz, S. Spatial Heterogeneity in the Mammalian Liver. *Nat. Rev. Gastroenterol. Hepatol.* **2019**, *16* (7), 395–410. https://doi.org/10.1038/s41575-019-0134-x.
(14) Keller, P. J.; Ahrens, M. B. Visualizing Whole-Brain Activity and Development at the Single-Cell Level Using Light-Sheet Microscopy. *Neuron* **2015**, *85* (3), 462–483. https://doi.org/10.1016/j.neuron.2014.12.039.
(15) Kurashima, Y.; Tokuhara, D.; Kamioka, M.; Inagaki, Y.; Kiyono, H. Intrinsic Control of Surface Immune and Epithelial Homeostasis by Tissue-Resident Gut Stromal Cells. *Front. Immunol.* **2019**, *10*. https://doi.org/10.3389/fimmu.2019.01281.
(16) Zhuang, H.; Alavi, A. 18-Fluorodeoxyglucose Positron Emission Tomographic Imaging in the Detection and Monitoring of Infection and Inflammation. *Semin. Nucl. Med.* **2002**, *32* (1), 47–59. https://doi.org/10.1053/snuc.2002.29278.
(17) Robey, I. F.; Stephen, R. M.; Brown, K. S.; Baggett, B. K.; Gatenby, R. A.; Gillies, R. J. Regulation of the Warburg Effect in Early-Passage Breast Cancer Cells. *Neoplasia N. Y. N* **2008**, *10* (8), 745–756.
(18) Malham, M.; Hess, S.; Nielsen, R. G.; Husby, S.; Høilund-Carlsen, P. F. PET/CT in the Diagnosis of Inflammatory Bowel Disease in Pediatric Patients: A Review. *Am. J. Nucl. Med. Mol. Imaging* **2014**, *4* (3), 225–230.
(19) Frees, A. E.; Rajaram, N.; Iii, S. S. M.; Fontanella, A. N.; Dewhirst, M. W.; Ramanujam, N. Delivery-Corrected Imaging of Fluorescently-Labeled Glucose Reveals Distinct Metabolic Phenotypes in Murine Breast Cancer. *PLOS ONE* **2014**, *9* (12), e115529. https://doi.org/10.1371/journal.pone.0115529.
(20) Nitin, N.; Carlson, A. L.; Muldoon, T.; El-Naggar, A. K.; Gillenwater, A.; Richards-Kortum, R. Molecular Imaging of Glucose Uptake in Oral Neoplasia Following Topical Application of Fluorescently Labeled Deoxy-Glucose. *Int. J. Cancer J. Int. Cancer* **2009**, *124* (11), 2634–2642. https://doi.org/10.1002/ijc.24222.
(21) Langsner, R. J.; Middleton, L. P.; Sun, J.; Meric-Bernstam, F.; Hunt, K. K.; Drezek, R. A.; Yu, T. K. Wide-Field Imaging of Fluorescent Deoxy-Glucose in Ex Vivo Malignant and Normal Breast Tissue. *Biomed. Opt. Express* **2011**, *2* (6), 1514–1523. https://doi.org/10.1364/BOE.2.001514.
(22) Hu, F.; Chen, Z.; Zhang, L.; Shen, Y.; Wei, L.; Min, W. Vibrational Imaging of Glucose Uptake Activity in Live Cells and Tissues by Stimulated Raman Scattering. *Angew. Chem. Int. Ed.* **2015**, *54* (34), 9821–9825. https://doi.org/10.1002/anie.201502543.
(23) Long, R.; Zhang, L.; Shi, L.; Shen, Y.; Hu, F.; Zeng, C.; Min, W. Two-Color Vibrational Imaging of Glucose Metabolism Using Stimulated Raman Scattering. *Chem. Commun.* **2017**, *54* (2), 152–155. https://doi.org/10.1039/C7CC08217G.
(24) Quinn, G. P.; Keough, M. J. *Experimental Design and Data Analysis for Biologists*; Cambridge University Press: 265-274, 2002.
(25) Sullivan Lisa M. Repeated Measures. *Circulation* **2008**, *117* (9), 1238–1243. https://doi.org/10.1161/CIRCULATIONAHA.107.654350.
(26) MacIver, N. J.; Jacobs, S. R.; Wieman, H. L.; Wofford, J. A.; Coloff, J. L.; Rathmell, J. C. Glucose Metabolism in Lymphocytes Is a Regulated Process with Significant Effects on Immune Cell Function and Survival. *J. Leukoc. Biol.* **2008**, *84* (4), 949–957. https://doi.org/10.1189/jlb.0108024.
(27) Jacobs, S. R.; Herman, C. E.; MacIver, N. J.; Wofford, J. A.; Wieman, H. L.; Hammen, J. J.; Rathmell, J. C. Glucose Uptake Is Limiting in T Cell Activation and Requires CD28-

Mediated Akt-Dependent and Independent Pathways. *J. Immunol.* **2008**, *180* (7), 4476–4486. https://doi.org/10.4049/jimmunol.180.7.4476.
(28) Krawczyk, C. M.; Holowka, T.; Sun, J.; Blagih, J.; Amiel, E.; DeBerardinis, R. J.; Cross, J. R.; Jung, E.; Thompson, C. B.; Jones, R. G.; Pearce, E. J. Toll-like Receptor–Induced Changes in Glycolytic Metabolism Regulate Dendritic Cell Activation. *Blood* **2010**, *115* (23), 4742–4749. https://doi.org/10.1182/blood-2009-10-249540.
(29) Rodríguez-Prados, J.-C.; Través, P. G.; Cuenca, J.; Rico, D.; Aragonés, J.; Martín-Sanz, P.; Cascante, M.; Boscá, L. Substrate Fate in Activated Macrophages: A Comparison between Innate, Classic, and Alternative Activation. *J. Immunol.* **2010**, *185* (1), 605–614. https://doi.org/10.4049/jimmunol.0901698.
(30) van der Windt, G. J. W.; Everts, B.; Chang, C.-H.; Curtis, J. D.; Freitas, T. C.; Amiel, E.; Pearce, E. J.; Pearce, E. L. Mitochondrial Respiratory Capacity Is A Critical Regulator Of CD8+ T Cell Memory Development. *Immunity* **2012**, *36* (1), 68–78. https://doi.org/10.1016/j.immuni.2011.12.007.
(31) Cahalan, M. D.; Parker, I.; Wei, S. H.; Miller, M. J. Two-Photon Tissue Imaging: Seeing the Immune System in a Fresh Light. *Nat. Rev. Immunol.* **2002**, *2* (11), 872–880. https://doi.org/10.1038/nri935.
(32) Cahalan, M. D.; Parker, I. Choreography of Cell Motility and Interaction Dynamics Imaged by Two-Photon Microscopy in Lymphoid Organs. *Annu. Rev. Immunol.* **2008**, *26* (1), 585–626. https://doi.org/10.1146/annurev.immunol.24.021605.090620.
(33) Germain, R. N.; Bajénoff, M.; Castellino, F.; Chieppa, M.; Egen, J. G.; Huang, A. Y. C.; Ishii, M.; Koo, L. Y.; Qi, H. Making Friends in Out-of-the-Way Places: How Cells of the Immune System Get Together and How They Conduct Their Business as Revealed by Intravital Imaging. *Immunol. Rev.* **2008**, *221* (1), 163–181. https://doi.org/10.1111/j.1600-065X.2008.00591.x.
(34) Mueller, S. N.; Germain, R. N. Stromal Cell Contributions to the Homeostasis and Functionality of the Immune System. *Nat. Rev. Immunol.* **2009**, *9* (9), 618–629. https://doi.org/10.1038/nri2588.
(35) Sengupta, S.; Vitale, R. J.; Chilton, P. M.; Mitchell, T. C. Adjuvant Induced Glucose Uptake by Activated T Cells Is Not Correlated with Increased Survival. In *Oxygen Transport to Tissue XXIX*; Kang, K. A., Harrison, D. K., Bruley, D. F., Eds.; Advances In Experimental Medicine And Biology; Springer US: Boston, MA, 2008; pp 65–72. https://doi.org/10.1007/978-0-387-74911-2_8.
(36) Tennant, D. A.; Durán, R. V.; Gottlieb, E. Targeting Metabolic Transformation for Cancer Therapy. *Nat. Rev. Cancer* **2010**, *10* (4), 267–277. https://doi.org/10.1038/nrc2817.
(37) Weyand, C. M.; Goronzy, J. J. Immunometabolism in Early and Late Stages of Rheumatoid Arthritis. *Nat. Rev. Rheumatol.* **2017**, *13* (5), 291–301. https://doi.org/10.1038/nrrheum.2017.49.
(38) Sukumar, M.; Liu, J.; Ji, Y.; Subramanian, M.; Crompton, J. G.; Yu, Z.; Roychoudhuri, R.; Palmer, D. C.; Muranski, P.; Karoly, E. D.; Mohney, R. P.; Klebanoff, C. A.; Lal, A.; Finkel, T.; Restifo, N. P.; Gattinoni, L. Inhibiting Glycolytic Metabolism Enhances CD8+ T Cell Memory and Antitumor Function. *J. Clin. Invest.* **2013**, *123* (10), 4479–4488. https://doi.org/10.1172/JCI69589.
(39) Chang, C.-H.; Pearce, E. L. Emerging Concepts of T Cell Metabolism as a Target of Immunotherapy. *Nat. Immunol.* **2016**, *17* (4), 364–368. https://doi.org/10.1038/ni.3415.

(40) Willard-Mack, C. L. Normal Structure, Function, and Histology of Lymph Nodes. *Toxicol. Pathol.* **2006**, *34* (5), 409–424. https://doi.org/10.1080/01926230600867727.
(41) Gerner, M. Y.; Kastenmuller, W.; Ifrim, I.; Kabat, J.; Germain, R. N. Histo-Cytometry: A Method for Highly Multiplex Quantitative Tissue Imaging Analysis Applied to Dendritic Cell Subset Microanatomy in Lymph Nodes. *Immunity* **2012**, *37* (2), 364–376. https://doi.org/10.1016/j.immuni.2012.07.011.
(42) Belanger, M. C.; Kinman, A. W. L.; Catterton, M. A.; Ball, A. G.; Groff, B. D.; Melchor, S. J.; Lukens, J. R.; Ross, A. E.; Pompano, R. R. Acute Lymph Node Slices Are a Functional Model System to Study Immunity Ex Vivo. *bioRxiv* **2019**, 865543. https://doi.org/10.1101/865543.
(43) Ross, A. E.; Belanger, M. C.; Woodroof, J. F.; Pompano, R. R. Spatially Resolved Microfluidic Stimulation of Lymphoid Tissue Ex Vivo. *Analyst* **2017**, *142* (4), 649–659. https://doi.org/10.1039/C6AN02042A.
(44) Groff, B. D.; Kinman, A. W. L.; Woodroof, J. F.; Pompano, R. R. Immunofluorescence Staining of Live Lymph Node Tissue Slices. *J. Immunol. Methods* **2019**, *464*, 119–125. https://doi.org/10.1016/j.jim.2018.10.010.
(45) Kinman, A. W. L.; Pompano, R. R. Optimization of Enzymatic Antibody Fragmentation for Yield, Efficiency, and Binding Affinity. *Bioconjug. Chem.* **2019**, *30* (3), 800–807. https://doi.org/10.1021/acs.bioconjchem.8b00912.
(46) Schindelin, J.; Arganda-Carreras, I.; Frise, E.; Kaynig, V.; Longair, M.; Pietzsch, T.; Preibisch, S.; Rueden, C.; Saalfeld, S.; Schmid, B.; Tinevez, J.-Y.; White, D. J.; Hartenstein, V.; Eliceiri, K.; Tomancak, P.; Cardona, A. Fiji: An Open-Source Platform for Biological-Image Analysis. *Nat. Methods* **2012**, *9* (7), 676–682. https://doi.org/10.1038/nmeth.2019.
(47) Hughes, L. D.; Rawle, R. J.; Boxer, S. G. Choose Your Label Wisely: Water-Soluble Fluorophores Often Interact with Lipid Bilayers. *PLOS ONE* **2014**, *9* (2), e87649. https://doi.org/10.1371/journal.pone.0087649.
(48) Zou, C.; Wang, Y.; Shen, Z. 2-NBDG as a Fluorescent Indicator for Direct Glucose Uptake Measurement. *J. Biochem. Biophys. Methods* **2005**, *64* (3), 207–215. https://doi.org/10.1016/j.jbbm.2005.08.001.
(49) Xia, C.-Q.; Chernatynskaya, A. V.; Looney, B.; Wan, S.; Clare-Salzler, M. J. Anti-CD3 Antibody Treatment Induces Hypoglycemia and Super Tolerance to Glucose Challenge in Mice through Enhancing Glucose Consumption by Activated Lymphocytes. *J. Immunol. Res.* **2014**, *2014*.
(50) Chen, Y.; Zhang, J.; Zhang, X. 2-NBDG as a Marker for Detecting Glucose Uptake in Reactive Astrocytes Exposed to Oxygen-Glucose Deprivation In Vitro. *J. Mol. Neurosci.* **2015**, *55* (1), 126–130. https://doi.org/10.1007/s12031-014-0385-5.
(51) Folgmann, D. Optimized Protocol for Measuring 2-NBDG Uptake as a Cellular Marker of Glycolytic Demand. *Biomed. Eng. Undergrad. Honors Theses* **2016**.
(52) Liu, H.; Rhodes, M.; Wiest, D. L.; Vignali, D. A. A. On the Dynamics of TCR:CD3 Complex Cell Surface Expression and Downmodulation. *Immunity* **2000**, *13* (5), 665–675. https://doi.org/10.1016/S1074-7613(00)00066-2.
(53) Berglund, E. D.; Li, C. Y.; Poffenberger, G.; Ayala, J. E.; Fueger, P. T.; Willis, S. E.; Jewell, M. M.; Powers, A. C.; Wasserman, D. H. Glucose Metabolism In Vivo in Four Commonly Used Inbred Mouse Strains. *Diabetes* **2008**, *57* (7), 1790–1799. https://doi.org/10.2337/db07-1615.

(54) Blodgett, A. B.; Kothinti, R. K.; Kamyshko, I.; Petering, D. H.; Kumar, S.; Tabatabai, N. M. A Fluorescence Method for Measurement of Glucose Transport in Kidney Cells. *Diabetes Technol. Ther.* **2011**, *13* (7), 743–751. https://doi.org/10.1089/dia.2011.0041.
(55) Ball, S. W.; Bailey, J. R.; Stewart, J. M.; Vogels, C. M.; Westcott, S. A. A Fluorescent Compound for Glucose Uptake Measurements in Isolated Rat Cardiomyocytes. *Can. J. Physiol. Pharmacol.* **2002**, *80* (3), 205–209. https://doi.org/10.1139/y02-043.
(56) Bashkatov, A. N.; Genina, E. A.; Tuchin, V. V. Measurement of Glucose Diffusion Coefficients in Human Tissues; 2008. https://doi.org/10.1201/9781584889755.ch19.
(57) Girard, J.-P.; Moussion, C.; Förster, R. HEVs, Lymphatics and Homeostatic Immune Cell Trafficking in Lymph Nodes. *Nat. Rev. Immunol.* **2012**, *12* (11), 762–773. https://doi.org/10.1038/nri3298.
(58) Roos, D.; Loos, J. A. Changes in the Carbohydrate Metabolism of Mitogenicellay Stimulated Human Peripheral Lymphocytes I. Stimulation by Phytohaemagglutinin. *Biochim. Biophys. Acta BBA - Gen. Subj.* **1970**, *222* (3), 565–582. https://doi.org/10.1016/0304-4165(70)90182-0.
(59) Chen, H. W.; Heiniger, H. J.; Kandutsch, A. A. Relationship between Sterol Synthesis and DNA Synthesis in Phytohemagglutinin-Stimulated Mouse Lymphocytes. *Proc. Natl. Acad. Sci.* **1975**, *72* (5), 1950–1954. https://doi.org/10.1073/pnas.72.5.1950.
(60) Potter, M. R.; Moore, M. PHA Stimulation of Separated Human Lymphocyte Populations. *Clin. Exp. Immunol.* **1975**, *21* (3), 456–467.
(61) Movafagh, A.; Heydary, H.; Mortazavi-Tabatabaei, S. A.; Azargashb, E. The Significance Application of Indigenous Phytohemagglutinin (PHA) Mitogen on Metaphase and Cell Culture Procedure. *Iran. J. Pharm. Res. IJPR* **2011**, *10* (4), 895–903.
(62) Macintyre, A. N.; Gerriets, V. A.; Nichols, A. G.; Michalek, R. D.; Rudolph, M. C.; Deoliveira, D.; Anderson, S. M.; Abel, E. D.; Chen, B. J.; Hale, L. P.; Rathmell, J. C. The Glucose Transporter Glut1 Is Selectively Essential for CD4 T Cell Activation and Effector Function. *Cell Metab.* **2014**, *20* (1), 61–72. https://doi.org/10.1016/j.cmet.2014.05.004.
(63) Nista, A.; De Martino, C.; Malorni, W.; Marcante, M. L.; Silvestrini, B.; Floridi, A. Effect of Lonidamine on the Aerobic Glycolysis of Normal and Phytohemagglutinin-Stimulated Human Peripheral Blood Lymphocytes. *Exp. Mol. Pathol.* **1985**, *42* (2), 194–205. https://doi.org/10.1016/0014-4800(85)90027-9.